ACS OMEGA

http://pubs.acs.org/journal/acsodf

Article

Core–Shell ZIF67@ZIF8 Modified with Phytic Acid as an Effective Flame Retardant for Improving the Fire Safety of Epoxy Resins

Hongni Wang, Xiaoqian Li, Fangfang Su, Jinliang Xie, Yangyang Xin, Weirui Zhang, Chen Liu, Dongdong Yao,* and Yaping Zheng*

Cite This: *ACS Omega* 2022, 7, 21664–21674

Read Online

ACCESS | Metrics & More | Article Recommendations | Supporting Information

ABSTRACT: Despite many important industrial applications, epoxy resin (EP) suffers from high flammability and toxicity emission, extremely hampering their applications. To circumvent the problem, core–shell structured ZIF67@ZIF8 is successfully synthesized and further functionalized with phytic acid (PA) to obtain PA-ZIF67@ZIF8 hybrids. Then, it is used as an efficient flame retardant to reduce the fire risk of EP. The fire test results show a significant reduction in heat and smoke production. Compared with EP, incorporating 5.0 wt % PA-ZIF67@ZIF8 into EP, the peak heat release rate, total heat release, and peak carbon monoxide production are dramatically reduced by 42.2, 33.0, and 41.5%, respectively. Moreover, the EP/PA-ZIF67@ZIF8 composites achieve the UL-94 V-0 rating and the limiting oxygen index increases by 29.3%. These superior fire safety properties are mainly attributed to the excellent dispersion and the catalytic effect of metal oxide and phosphorus-containing compounds. This work provides an efficient strategy for preparing a promising ZIF-based flame retardant for enhancing flame retardancy and smoke toxicity suppression of EP.

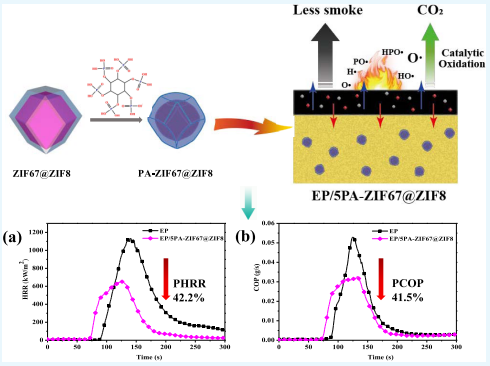

1. INTRODUCTION

Epoxy resin (EP) is one of the promising thermosetting polymers. It has been extensively used in many fields, such as painting, building construction, and composite applications, owing to its high thermal stability, outstanding mechanical properties, and excellent chemical resistance.[1−4] However, its inflammability severely poses many disadvantages for its applications.[5,6] Hence, it is imperative to improve the fire-retardant performance of EP.

Metal–organic frameworks (MOFs) are a kind of porous material consisting of metal ions (or metal clusters) and organic linkers.[7] They have been widely used in the fields of gas separation, drug delivery, proton conductivity, etc.[8,9] Recently, MOFs have attracted increasing attention in fire retardancy studies.[10−13] Compared with traditional flame retardants (FRs), MOFs exhibit superior compatibility with polymers due to the existence of organic linkers.[14−16] Here, it should be mentioned that the zeolitic imidazolate frameworks (ZIFs) are a subset of MOFs, which are composed of metal ions and imidazolate ligands.[17,18] The ZIFs commonly used as FRs are the Co^{2+}-containing zeolitic imidazolate framework (ZIF67) and Zn^{2+}-containing zeolitic imidazolate framework (ZIF8), which contain abundant flame-retardant elements. The metallic element can work with the nitrogen element to improve the fire safety of polymers together.[11,14,19] For example, Xu et al.[20] added a ZIF8/reduced graphene oxide hybrid in the EP matrix to decrease the peak heat release rate (PHRR) and total smoke production (TSP) of EP by 65 and 36.8%, respectively. In addition, Li et al.[21] designed a ZIF67@MgAl-LDH hybrid to improve the performance of EP with a decrease in the total heat release rate of 39.3% and TSP of 38%.

However, it is difficult to achieve the desired flame-retardant effect by alternatively adding ZIF67 or ZIF8 to the polymer matrix. To solve the limitations of ZIF67 and ZIF8 flame retardance, bimetallic (Zn and Co) ZIF derivatives are prepared to improve the flame retardancy of polymeric materials. For example, Hou et al.[22] used bimetallic ZIF derivatives (ZIF67 and ZIF8) as sacrificial agents to synthesize Co–Ni LDHs on the surfaces of GO or CNTs, and the UPR composites exhibit excellent flame retardancy as expected. At a loading amount of 2 wt %, UPR composites exhibit 27.7 and 22.7% decreases in the value of TSP. Zhang et al.[14] synthesized Zn and Co bimetallic ZIFs on the surface of GO to improve the fire safety of EP. With the addition of 2 wt % MOF@GO, the PHRR of EP nanocomposites decreased by 29.4%. However, according to previous reports, the sample consisting of two different nanoparticles by physical mixing shows a poor flame-retardant effect than that of corresponding core–shell

Received: March 15, 2022
Accepted: May 19, 2022
Published: June 14, 2022

Scheme 1. Synthesis Route of ZIF67@ZIF8 and PA-ZIF67@ZIF8

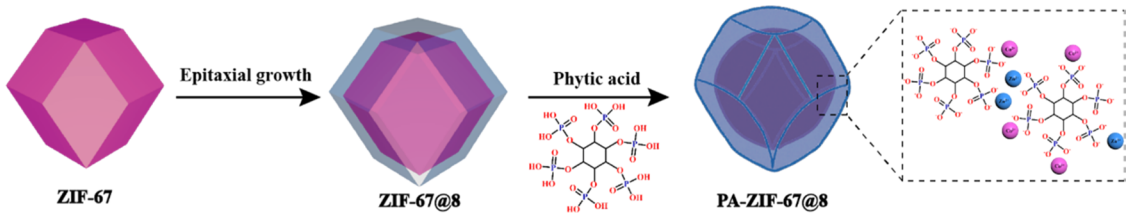

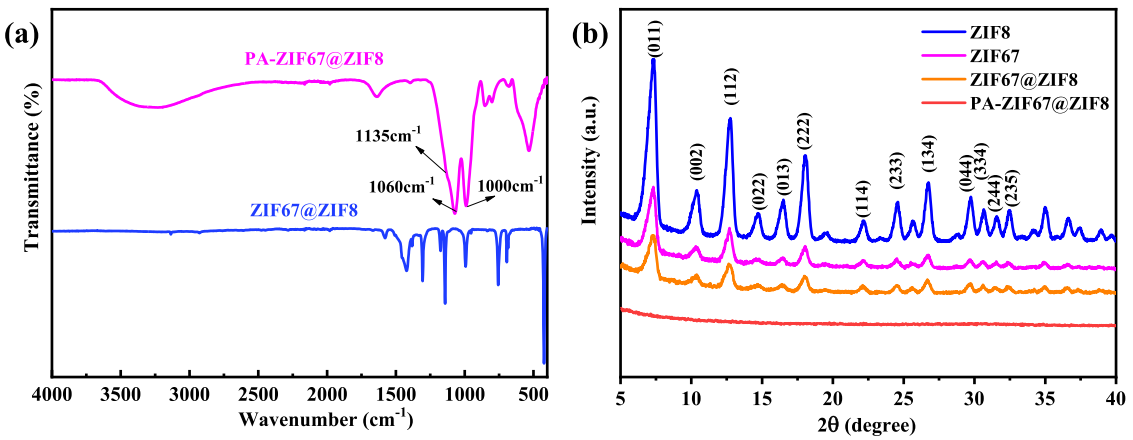

Figure 1. (a) FTIR spectra and (b) XRD patterns of ZIF67@ZIF8 and ZIF67@ZIF8-PA.

structured nanohybrid particles. For instance, EP/6ZHS@NCH shows a higher LOI value than EP/6(ZHS + NCH).[23] The EP/MOF@GO and EP/MOF-GO show the same results.[14] Hence, core−shell structured ZIF67@ZIF8 was synthesized and prepared.[24,25] Until now, the utilization of ZIF67@ZIF8 and its derivatives as flame retardants has not been reported.

To further improve the flame retardancy of ZIF67@ZIF8, it is necessary to functionalize ZIF67@ZIF8. Among all halogen-free flame retardants, phosphorus-containing flame retardants are one of the most promising candidates because of their low toxicity, high efficiency, and multiple flame retardancy mechanisms.[26−29] Phytic acid (PA), as an environmentally friendly and biocompatible organic acid, has gained increasing interest as an effective flame retardant due to the abundance of phosphorus (28% P).[30−32]

In this study, phytic acid was employed to functionalize ZIF67@ZIF8 to form core−shell structured ZIF67@ZIF8-PA hybrids and ZIF67@ZIF8-PA hybrids were then added to the EP matrix via a physical blending method. The thermal stabilities and fire hazards of the EP composites were investigated systematically. Furthermore, the flame retardancy mechanism of EP composites was proposed.

2. EXPERIMENTAL SECTION

2.1. Materials. Cobalt(II) nitrate hexahydrate ($Co(NO_3)_2·6H_2O$) and 2-methylimidazole (2-MIM) were purchased from Macklin Biochemical Co., Ltd. (Shanghai, China). Zinc nitrate hexahydrate ($Zn(NO_3)_2·6H_2O$) was bought from Sinopharm Chemical Reagent Co., Ltd. (Shanghai, China). Diamino diphenylmethane (DDM) and phytic acid (50% in H_2O) were provided by Aladdin Chemistry Co., Ltd. (Shanghai, China). EP (E-51) was obtained from Petrochemical Co., Ltd. (Yueyang, Hunan).

2.2. Preparation of ZIF67@ZIF8. $Co(NO_3)_2·6H_2O$ (10.92 g) and 2-methylimidazole (12.32 g) were dissolved in 100 mL of methanol and 150 mL of methanol, respectively. Then, the $Co(NO_3)_2·6H_2O$ solution was added dropwise to the 2-methylimidazole solution under ultrasonication. After that, $Zn(NO_3)_2·6H_2O$ (12.32 g) in 100 mL of methanol was slowly added to the mixture and exposed to ultrasonic treatment for another 1 h, followed by stirring for 12 h at room temperature. Finally, the crude was washed with methanol and dried at 80 °C for 12 h. The preparation diagram of ZIF67@ZIF8 and PA-ZIF67@ZIF8 is displayed in Scheme 1.

2.3. Preparation of PA-ZIF67@ZIF8. In a typical procedure, 1 g of ZIF67@ZIF8 was dispersed into 150 mL of deionized water under sonication. PA solution (2.5 g) was added slowly to the suspensions above. The reaction would occur for 24 h with constant stirring at room temperature. Subsequently, the products were washed thoroughly with distilled water several times and then dried at 80 °C for 10 h.

2.4. Preparation of EP Composites. The fabrication procedure of EP composites containing 2 wt % ZIF67@ZIF8 was performed as follows: 1.2 g of ZIF67@ZIF8 and 11.76 g of DDM were dispersed into acetone by sonication. Then, 47.04 g of EP was added to the suspension with mechanical stirring for 2 h to obtain a uniform system. Whereafter, the mixture was transferred into a vacuum oven at 50 °C for 2 h to remove the acetone. Finally, the mixture was poured into a prepared Teflon mold and cured at 100 and 150 °C for 2 h, respectively. The EP composite was successfully prepared after natural cooling to room temperature, where EP composites containing 2.0 and 5.0 wt % ZIF67@ZIF8 were designated as EP/2ZIF67@ZIF8 and EP/5ZIF67@ZIF8, respectively; they could be fabricated using the same procedure. To make a comparison, EP/2PA-ZIF67@ZIF8 and EP/5PA-ZIF67@

https://doi.org/10.1021/acsomega.2c01545
ACS Omega 2022, 7, 21664−21674

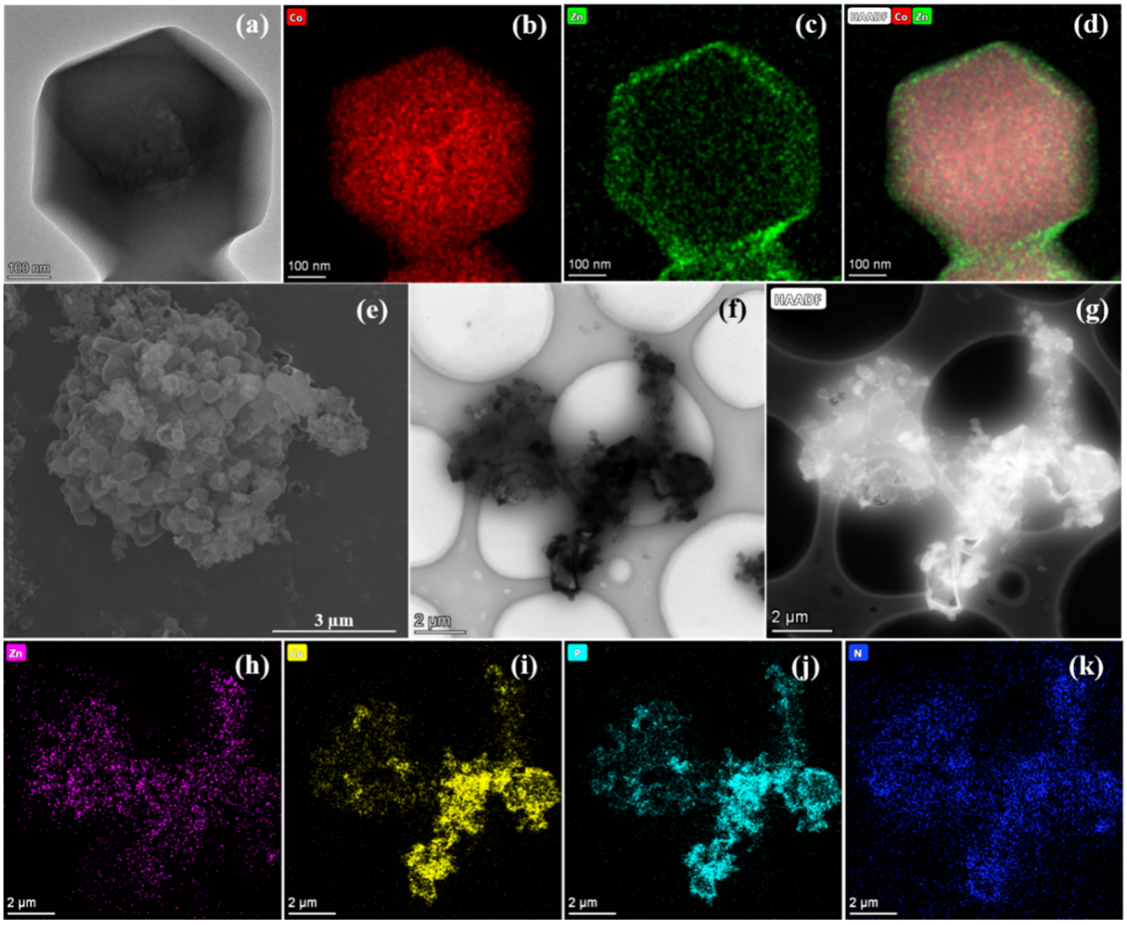

Figure 2. (a) TEM image of ZIF67@ZIF8 and corresponding elemental mapping of (b) Co, (c) Zn, and (d) the layered image of panels a−c, (e) SEM image of PA ZIF67@ZIF8, (f, g) TEM image of PA-ZIF67@ZIF8 and corresponding elemental mapping of (h) Zn, (i) Co, (j) P, and (k) N.

ZIF8 with 2.0 and 5.0 wt % PA-ZIF67@ZIF8 were prepared by the same approach.

2.5. Characterization. The detailed characterization is provided in the Supporting information.

3. RESULTS AND DISCUSSION

3.1. Characterization of ZIF67@ZIF8 and PA-ZIF67@ZIF8. Fourier transform infrared (FTIR) analysis provides the structural information of ZIF67@ZIF8 and PA-ZIF67@ZIF8. The FTIR spectra of ZIF67@ZIF8 and PA-ZIF67@ZIF8 are shown in Figure 1a. According to the FTIR spectrum of ZIF67@ZIF8, the typical peaks at 423 and 419 cm^{-1} are attributed to the stretching vibrations of Co−N and Zn−N, respectively.[16,20] The peak in the range of 500−1600 cm^{-1} is assigned to the typic stretching vibration of 2-methimidazole.[20] For PA-ZIF67@ZIF8, two newly emerged bands at 1130 and 1068 cm^{-1} are allocated to the stretching vibration of P−O and P═O, respectively,[32] while the peaks at 620 and 520 cm^{-1} are ascribed to the characteristic stretching vibrations of Co−O and Zn−O, respectively.[23] The crystal structures of ZIF67@ZIF8 and PA-ZIF67@ZIF8 are examined by the X-ray diffraction (XRD) technique. As shown in Figure 1b, the diffraction peaks of ZIF67@ZIF8 show a very close agreement with the XRD patterns of ZIF8 and ZIF67 as reported in the literature,[24,25] which is caused by the similar unit cell parameters of ZIF67 and ZIF8. However, after ZIF67@ZIF8 is functionalized with PA, the characteristic peaks of ZIF7@ZIF8 are not found because PA gradually breaks the coordination bonds of ZIF67@ZIF8.

The morphologies of ZIFs are studied by scanning electron microscopy (SEM) and transmission electron microscopy (TEM). As shown in Figure 2, ZIF67@ZIF8 exhibits a rhombic dodecahedral morphology and a diameter of ca. 500 nm. To further determine the core−shell structure of ZIF67@ZIF8, elemental analysis is performed by energy-dispersive X-ray spectroscopy (EDS) elemental mapping. It is observed that Co is situated at the center and Zn is distributed over the whole sample, indicating that the core−shell structure of ZIF67@ZIF8 is successfully synthesized. After further modification with PA, its morphology is quite distinct from that of ZIF67@ZIF8 (Figure 2e,f). From Figure 2h−k, the EDS results of PA-ZIF67@ZIF8 exhibit the target elements of Co, Zn, N, and P that are distributed homogeneously, which is consistent with the results of XPS analysis (Figure 3a).

XPS spectra are utilized to determine the chemical states and elemental compositions of ZIF67@ZIF8 and PA-ZIF67@ZIF8. As depicted in Figure 3a, the XPS spectrum of ZIF67@ZIF8 reveals the Co 2p, Zn 2p, and N 1s peaks. In comparison, PA-ZIF67@ZIF8 exhibits two new sharp peaks of P 2p (133.0 eV) and P 2s (189.0 eV).[32] Meanwhile, the peak of N 1s is significantly decreased, which is due to part of amine groups reacting with PA. In addition, the high-resolution N 1s, Co 2p, and Zn 2p XPS spectra of PA-ZIF67@ZIF8 are presented in Figure 3b,d. As for the N 1s spectrum, the peaks at 399 and 409.1 eV are assigned to Ph−NH_2 and −NH_3^+, respectively.[32]

https://doi.org/10.1021/acsomega.2c01545
ACS Omega 2022, 7, 21664−21674

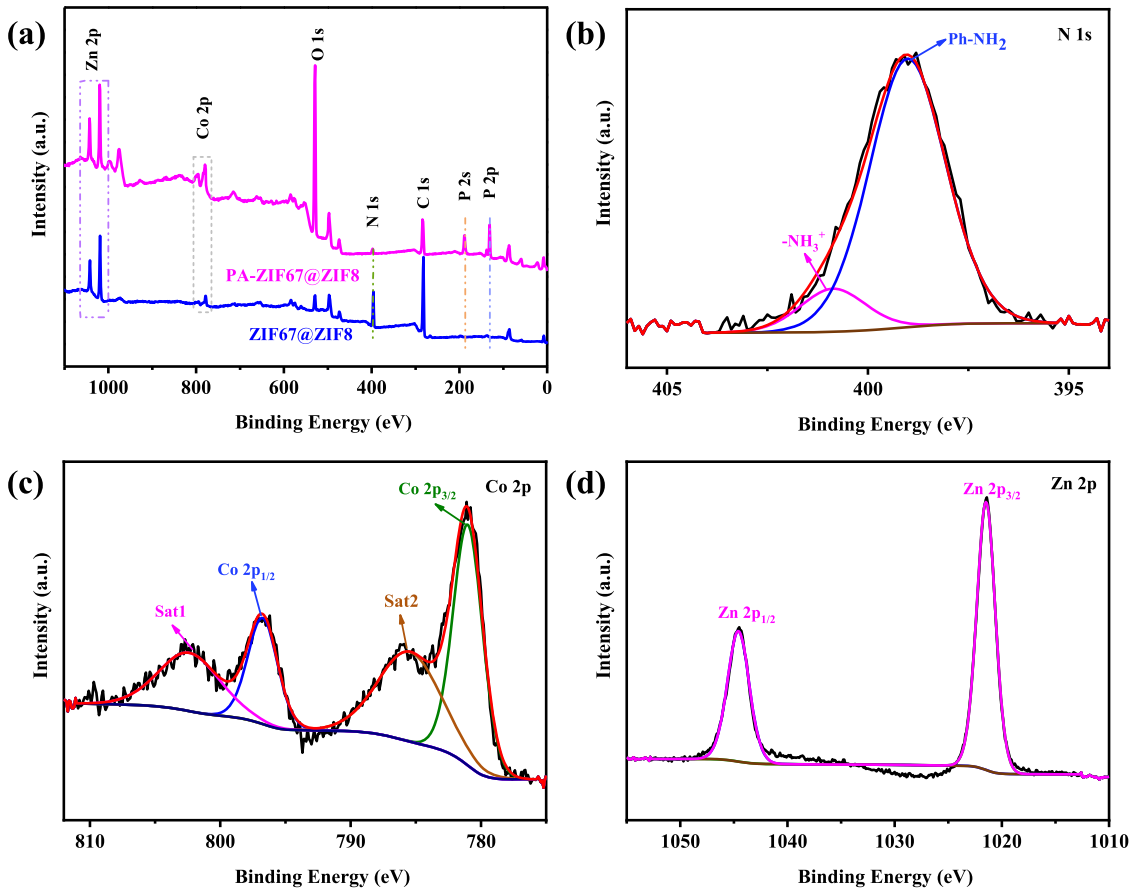

Figure 3. (a) XPS patterns of ZIF67@ZIF8 and PA-ZIF67@ZIF8 and high-resolution XPS spectra of (b) P 2p, (c) Co 2p, and (d) Zn 2p.

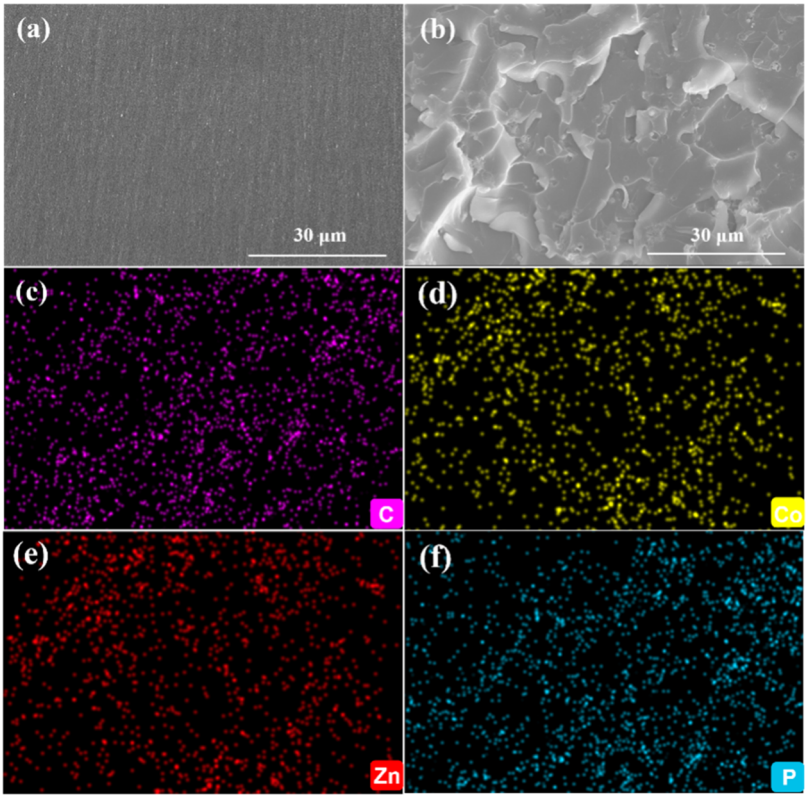

Figure 4. (a) SEM images of the fractured surfaces for (a) EP and (b) EP/5PA-ZIF67@ZIF8 and corresponding elemental mapping images of (c) C, (d) P, (e) Zn, and (f) Co.

https://doi.org/10.1021/acsomega.2c01545
ACS Omega 2022, 7, 21664−21674

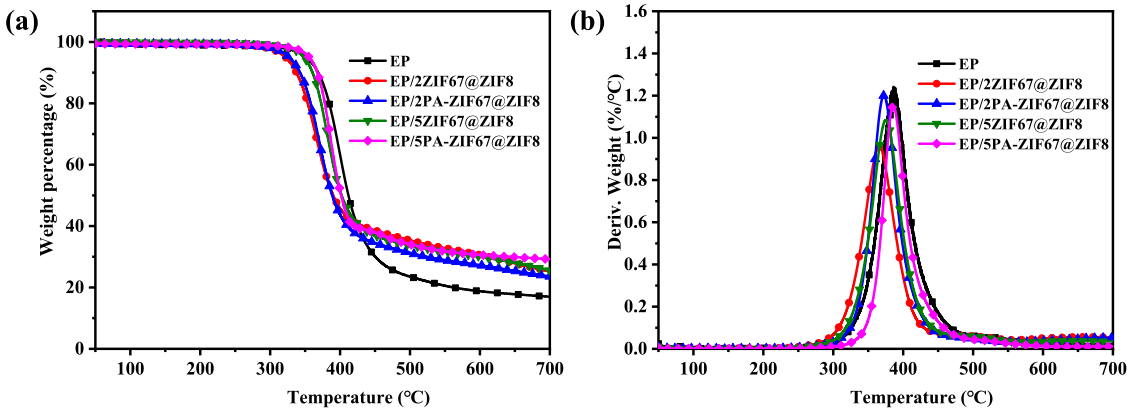

Figure 5. (a) TGA and (b) DTG curves of EP and its composites under a nitrogen atmosphere.

In the case of the Co 2p spectrum, besides two peaks centered at 781.1 eV (Co $2p_{3/2}$) and 797.1 eV (Co $2p_{1/2}$), there are two satellite peaks appearing at 786.1 eV (Co $2p_{3/2}$) and 803.1 eV (Co $2p_{1/2}$).[16] In the case of the Zn 2p spectrum, Zn $2p_{1/2}$ and Zn $2p_{3/2}$ are located at 1044.2 and 1021.2 eV, respectively.[23] These results confirm that the ZIF67@ZIF8 has been functionalized by PA.

3.2. Dispersion of PA-ZIF67@ZIF8 in the EP Matrix. The dispersion of EP/5PA-ZIF67@ZIF8 in the EP matrix is investigated by SEM. As shown in Figure 4a, the fractured surface of EP is smooth, while the fractured surface of EP/5PA-ZIF67@ZIF8 is relatively rough (Figure 4b). To further study the dispersion of EP/5PA-ZIF67@ZIF8, elemental analysis of the fracture surfaces is characterized by EDS. The corresponding mapping images of the fracture surface are shown in Figure 4c–f. The main C, P, Co, and Zn elements are evenly distributed on the fracture surface, demonstrating that 5 wt % PA-ZIF67@ZIF8 exhibits good dispersion in the epoxy matrix. Meanwhile, the dispersion of ZIF67@ZIF8 and PA-ZIF67@ZIF8 in EP is further characterized by TEM. TEM images of EP/5ZIF67@ZIF8 and EP/5PA-ZIF67@ZIF8 are shown in Figure S1. Obviously, ZIF67@ZIF8 and PA-ZIF67@ZIF8 are dispersed uniformly without aggregation in the EP matrix.

3.3. Thermal Behavior and Mechanical Properties of EP and Its Composites. The thermal property of EP composite samples in a N_2 atmosphere is displayed in Figure 5, and the corresponding data are listed in Table 1, where $T_{5\%}$ and T_{max} are defined as the temperature at 5 wt % weight loss and the maximum weight loss, respectively. As shown in Figure 5a, all EP composite samples display one-step mass loss in the N_2 atmosphere. The $T_{5\%}$ of EP/2ZIF67@ZIF8 and EP/5ZIF67@ZIF8 is reduced slightly to that of EP due to the catalytic decomposition of ZIF67@ZIF8. However, the $T_{5\%}$ of EP/2PA-ZIF67@ZIF8 and EP/5PA-ZIF67@ZIF8 is increased by 16 and 31 °C, respectively. Compared to that of EP, the T_{max} of the EP composites decreases slightly. Furthermore, compared with that of EP, the char yields of EP composites are increased. Particularly, the addition of 5 wt % PA-ZIF67@ZIF8 to EP improves the char residues from 17.0 to 29.2 wt %, indicating that the coordination of 5 wt % PA-ZIF67@ZIF8 can accelerate the formation of residual char. Figure 5b displays the derivative thermogravimetric analysis (DTG) curves of all EP composite samples; the maximum mass loss rates of EP composites are lower relative to those of EP, indicating that the thermal stability of EP composites is improved. The mechanical properties of EP and its composites are further studied by DMA. Figure S2 presents the storage modulus and tan delta of EP and EP composites as a function of temperature. With the addition of 5 wt % fillers, the storage modulus of EP composites at 40 °C is higher than that of EP. In particular, the storage modulus of EP/5PA-ZIF67@ZIF8 increases from 2340 to 2503 MPa. The glass transition temperature of each sample decreases compared with that of pure EP.

Table 1. TGA Data of EP Composite Samples

samples	$T_{5\%}$ (°C)	T_{max} (°C)	residue at 700 °C (%)
EP	320	387	17.0 ± 0.8
EP/2ZIF67@ZIF8	316	365	25.1 ± 0.7
EP/2PA-ZIF67@ZIF8	336	369	24.8 ± 0.4
EP/5ZIF67@ZIF8	319	377	26.1 ± 0.3
EP/5PA-ZIF67@ZIF8	351	385	29.2 ± 1.5

3.4. Fire Performance of EP and Its Composites. The relative combustibility of EP and its composites is assessed by the limiting oxygen index (LOI) and UL-94 vertical test, and the relevant data are summarized in Table 2. The LOI value of EP is 25.4% and no rating (NR) in the vertical UL-94 test. With the introduction of 2 wt % of ZIF67@ZIF8 and PA-ZIF67@ZIF8 into EP, the LOI values increase to 28.1 and 27.7%, respectively. In particular, when the content of ZIF67@ZIF8 and PA-ZIF67@ZIF8 increases to 5 wt %, the LOI values of EP/5ZIF67@ZIF8 and EP/5PA-ZIF67@ZIF8 enhance to

Table 2. Related Data of EP and Its Composites from UL-94, LOI, and CCT at 35 kW/m²

sample	UL-94 test	LOI (%)	PHRR (kW/m²)	THR (kW/m²)	TSP (m²)	PCOP (g/s)	av-EHC (MJ/K)	Char (wt %)
EP	NR	25.4 ± 0.2	1133.0 ± 52	92.2 ± 2.0	20.6 ± 1.2	0.053 ± 0.002	27.5 ± 1.5	11.4 ± 0.5
EP/2ZIF67@ ZIF8	V-1	28.1 ± 0.1	958.3 ± 41	73.8 ± 1.8	16.7 ± 0.7	0.039 ± 0.002	26.2 ± 0.8	13.5 ± 1.2
EP/2PA-ZIF67@ZIF8	V-1	27.7 ± 0.3	1078.9 ± 31	80.2 ± 0.7	17.2 ± 0.8	0.038 ± 0.001	26.9 ± 1.2	13.8 ± 2.1
EP/5ZIF67@ ZIF8	V-0	28.5 ± 0.2	700.6 ± 41	67.8 ± 1.2	15.4 ± 0.5	0.032 ± 0.002	24.7 ± 2.0	22.9 ± 1.7
EP/5PA-ZIF67@ZIF8	V-0	29.3 ± 0.4	651.5 ± 37	61.8 ± 3.2	15.0 ± 0.7	0.029 ± 0.002	23.2 ± 1.9	25.4 ± 1.3

https://doi.org/10.1021/acsomega.2c01545
ACS Omega 2022, 7, 21664−21674

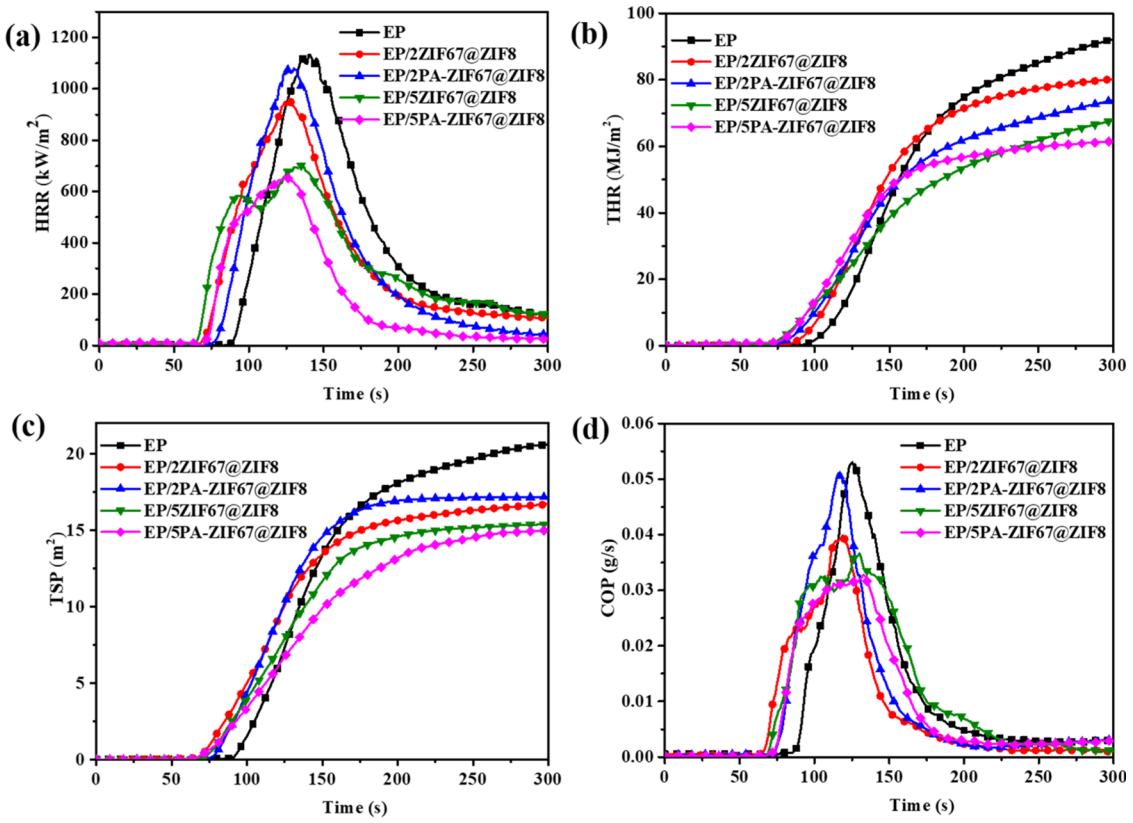

Figure 6. (a) HRR, (b) TSP, (c) TSP, and (d) COP curves of EP and its composites.

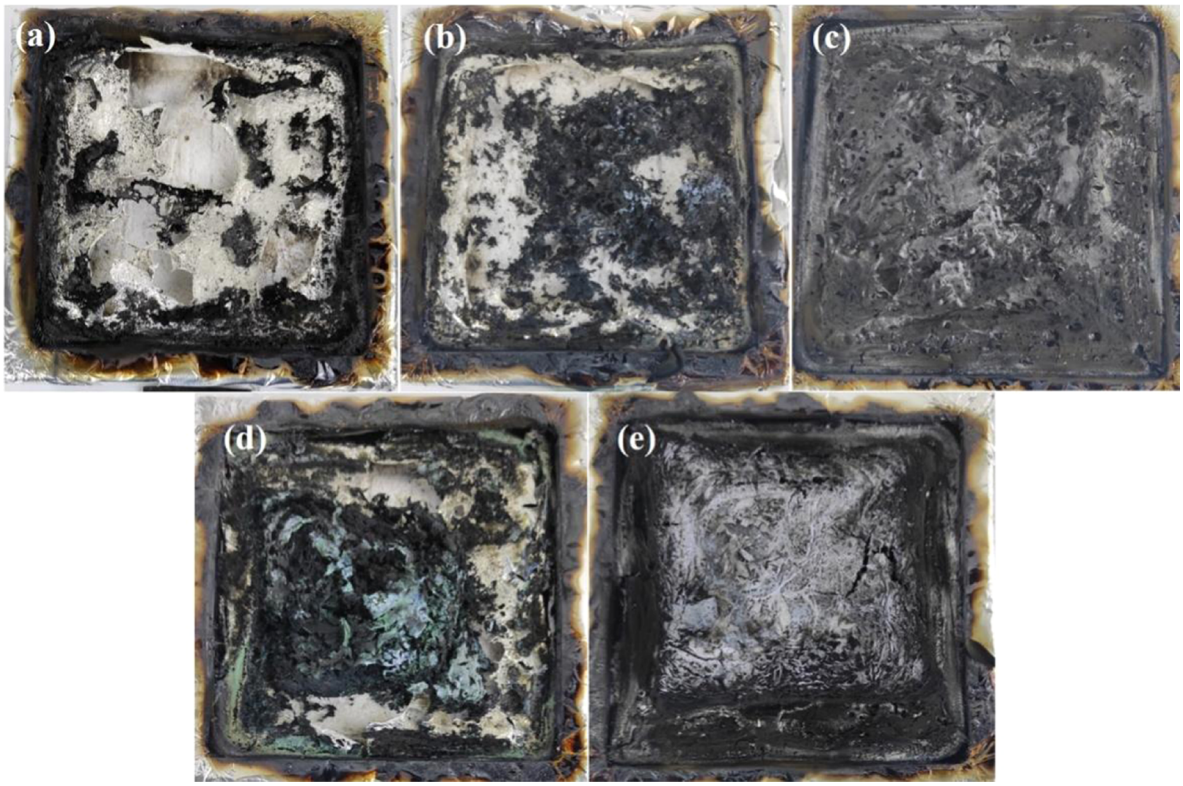

Figure 7. Digital images of the char residues for (a) EP, (b) EP/2ZIF67@ZIF8, (c) EP/2PA-ZIF67@ZIF8, (d) EP/5ZIF67@ZIF8, and (e) EP/5PA-ZIF67@ZIF8.

28.5 and 29.3%, respectively, and both samples pass the V-0 rating.

Based on LOI and UL-94 results, the fire behavior of EP and its composites is further studied by a cone calorimeter test at

https://doi.org/10.1021/acsomega.2c01545
ACS Omega 2022, 7, 21664−21674

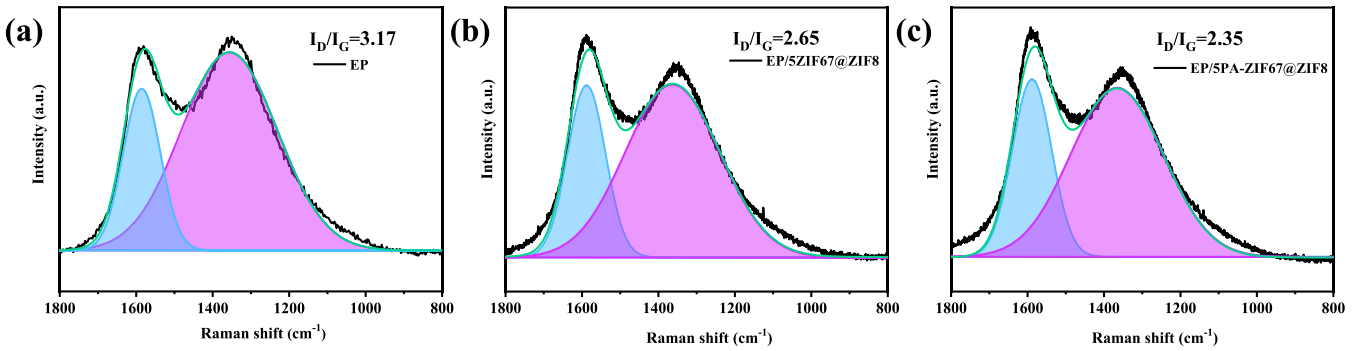

Figure 8. Raman spectra of char residues for (a) EP, (b) EP/5ZIF67@ZIF8, and (c) EP/5PA-ZIF67@ZIF8.

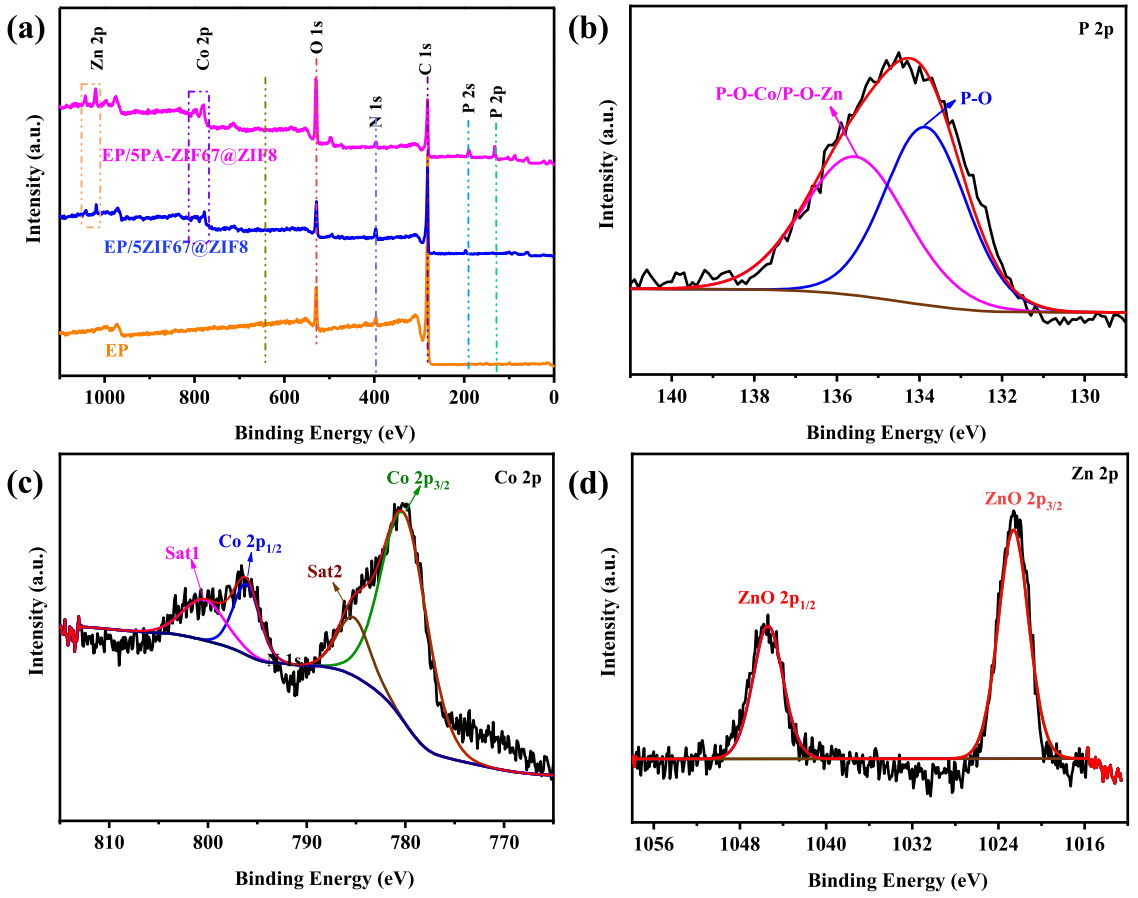

Figure 9. XPS spectra of the char residue for (a) EP, EP/5ZIF67@ZIF8 and EP/5PA-ZIF67@ZIF8 and high-resolution spectra of (b) P 2p, (c) Co 2p, and (d) Zn 2p in EP/5PA-ZIF67@ZIF8.

35 kW/m^2, and the detailed data are listed in Table 2. As shown in Figure 6a, EP burns fiercely and reaches a very high PHRR of 1133 kW m^{-2} in a short time, indicating that EP is highly flammable. When incorporating ZIF67@ZIF8 and PA-ZIF67@ZIF8, the PHRR values are reduced relative to pure EP. In addition, among all samples, EP/5PA-ZIF67@ZIF8 exhibits the lowest PHRR value, only 651.5 kW m^{-2}, which is decreased by 42.2%, demonstrating that PA can improve the retardancy of EP composites compared with that of only 5 wt % ZIF67@ZIF8. However, the fire behavior of EP/2PA-ZIF67@ZIF8 is worse than that of EP/2ZIF67@ZIF8, which is probably because phytic acid can lead to a positive effect on the flame-retardant properties of EP composites when it raises to a certain extent. As a result, the EP/5PA-ZIF67@ZIF8 exhibits a better fire performance than that of EP/5ZIF67@ZIF8. Figure 6b shows the THR curves for EP and its composites; the trend of THR is similar to that of HRR. The THR values are reduced from 92.2 MJ/m^2 of EP to 61.6 MJ/m^2 of EP/5PA-ZIF67@ZIF8 (33.2%). As mentioned above, the early decomposition of PA-ZIF67@ZIF8 contributes to accelerating the formation of a stable char layer, which serves as a physical barrier to protect the underlying matrix, thus resulting in the decrease of PHRR and THR. As shown in Table 2, EP/5PA-ZIF67@ZIF8 shows a lower average effective heat of combustion (av-EHC). The reduction of the EHC means fuel dilution and lower combustion heat generated during the burning.

https://doi.org/10.1021/acsomega.2c01545
ACS Omega 2022, 7, 21664−21674

Smoke and toxic fumes (e.g., CO) that are released are the other major causes of fatality in a real fire. Figure 6c,d displays the total smoke production (TSP) and carbon monoxide production (COP) curves of EP and its composites. As can be seen from Figure 6c, the TSP of EP reaches up to 20.6 m^2/s, while that of EP/5PA-ZIF67@ZIF8 reduces by 27.2% relative to EP. The peak carbon monoxide production (PCOP) of EP/5PA-ZIF67@ZIF8 is decreased by 41.5% compared with that of EP. Total CO production (TCOP) curves of the EP and its composites are shown in Figure S3; the TCOP of EP reaches up to 22.6 g, while EP/5PA-ZIF67@ZIF8 reduces by 37.7% relative to EP. Additionally, the char residue rate of EP with the combustion time of 600 s is 11.4%, and the char residue rate of EP/5PA-ZIF67@ZIF8 is increased to 25.4%, which is ca. 2.3 times the weight of EP. This is mainly because of the phosphorous moieties and metal oxides generated in the combustion process of PA-ZIF67@ZIF8, which can promote the formation of residue in the condensed phase.[30,33]

3.5. Analysis of Char Residues. To explore the flame retardancy mechanism, the residual char generated after the cone calorimeter is investigated. The char residues are not the fire residues during burning, and the residue does not show the carbonaceous char properly. However, it can explain the relationship between the char layer and the fire retardancy mechanism to a certain extent. The digital photos of the char residues for EP and its composites are taken with a digital camera and shown in Figure 7. EP is almost burnt out, and enormous pores form on the char surface, which was unable to serve as a protective layer. With the addition of 2 wt % ZIF67@ZIF8 and 2 wt % PA-ZIF67@ZIF8, the char yields are gradually increased compared with EP. Meanwhile, the pores on the char surface are fewer and smaller. Although EP/2PA-ZIF67@ZIF8 shows more char residue than EP/2ZIF67@ZIF8, the char residue for EP/2PA-ZIF67@ZIF8 displays a relatively fluffy structure with larger holes on the surface, that is why EP/2PA-ZIF67@ZIF8 exhibits worse fire behavior. In comparison, EP/5ZIF67@ZIF8 and EP/5PA-ZIF67@ZIF8 display a higher amount of char residues than EP/2ZIF67@ZIF8 and EP/2PA-ZIF67@ZIF8. Notably, EP/5PA-ZIF67@ZIF8 has the highest amount of char residue than that of the other samples; the char residue of EP/5PA-ZIF67@ZIF8 appears more continuous and shows a dense char layer than other samples.

The structure of char residues after the cone calorimetry test is investigated by Raman spectra. As shown in Figure 8, two strong characteristic peaks at ca. 1365 and 1600 cm^{-1} are assigned to the D (vibration of amorphous carbon) and G (vibration of crystalline carbon) bands.[34] Usually, the ratio of the band intensity of the D to G band (I_D/I_G) is used to estimate the graphitization degree of the char residues, and a lower value corresponds to a higher graphitization degree.[35] From Figure 8a, the I_D/I_G value of EP is the highest (3.17), whereas the I_D/I_G values of EP/5ZIF67@ZIF8 and EP/5PA-ZIF67@ZIF8 are lower than that of EP. Particularly, EP/5PA-ZIF67@ZIF8 exhibits the lowest I_D/I_G (2.35). It demonstrates that a more graphitized structure in char residue is formed during the combustion of EP/5PA-ZIF67@ZIF8, which can improve the insulation of fuel and heat transfer.

To further elucidate the formation of the char layer, the residual char for EP and its composite thermosets after cone calorimeter tests are examined by the XPS spectra and XRD spectra, as shown in Figures 9 and S2, respectively. The full XPS survey spectrum presents the existence of C, O, and N elements in the char residues for all of the samples. Besides these elements, the elements of Co and Zn are discovered in the char residues of EP/5ZIF67@ZIF8 and EP/5PA-ZIF67@ZIF8, whereas the P element only appears in the char layer of EP/5PA-ZIF67@ZIF8 due to the existence of PA in EP/5PA-ZIF67@ZIF8. The high-resolution XPS spectra of EP/5PA-ZIF67@ZIF8 are shown in Figure 9b–d. In the P 2p spectrum, the peaks at 133.8 and 135.4 eV correspond to P–O and P–O–Co/P–O–Zn, respectively.[30] Figure 9c shows the Co 2p spectrum; besides two satellite peaks of Co $2p_{3/2}$ (786.1 eV) and Co $2p_{1/2}$ (803.1 eV), two peaks appear at 781.1 and 797.1 eV, which are assigned to Co $2p_{3/2}$ and Co $2p_{1/2}$, respectively.[36] In the Zn 2p spectrum, two major peaks at 1022.1 and 1045.4 eV are attributed to the Zn–O bond.[13] These results demonstrate that Co_3O_4, ZnO, and phosphoric acid or polyphosphoric acid generated during the burning process of PA-ZIF67@ZIF8 can catalyze the formation of the char layer during burning. That is why the char layer of EP/5PA-ZIF67@ZIF8 is denser than other samples. XRD spectra of the char layer for EP/PA-ZIF67@ZIF8 are shown in S4, which can further prove the existence of Co_3O_4 and ZnO in the char layer.

3.6. Analysis of Volatile Gases. To study the influence of PA-ZIF67@ZIF8 on the pyrolysis gaseous products during the thermal decomposition process, TG-FTIR is performed to characterize the evolved gas products of EP and EP/5PA-ZIF67@ZIF8. The spectra at the maximum degradation rate of EP and EP/5PA-ZIF67@ZIF8 are presented in Figure 10. The

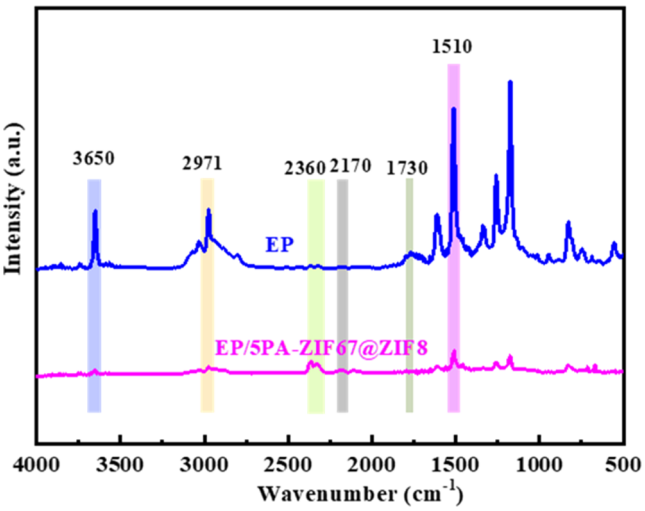

Figure 10. FTIR spectra of volatile gas emitted from EP and EP/5PA-ZIF67@ZIF8 at the maximum degradation rate.

characteristic peaks at 3650, 2971, 2360, 2180, 1730, and 1520 cm^{-1} are associated with –OH, aliphatic compound, CO_2, CO, carbonyl compounds, and aromatic compounds, respectively. As shown in Figure 11a–d, the absorbance intensity of pyrolysis products for EP/5PA-ZIF67@ZIF8 is decreased in comparison with that of EP, including aliphatic compounds, carbonyl compounds, and aromatic compounds. In particular, aliphatic compounds, carbonyl compounds, and aromatic compounds are the fuel supplies for combustion. The absorbance intensity of these compounds decreased, demonstrating that the fuel supplied for burning decreased. These organic compounds remained in the condensed phase, protecting the underlying polymers. It demonstrates that the

https://doi.org/10.1021/acsomega.2c01545
ACS Omega 2022, 7, 21664–21674

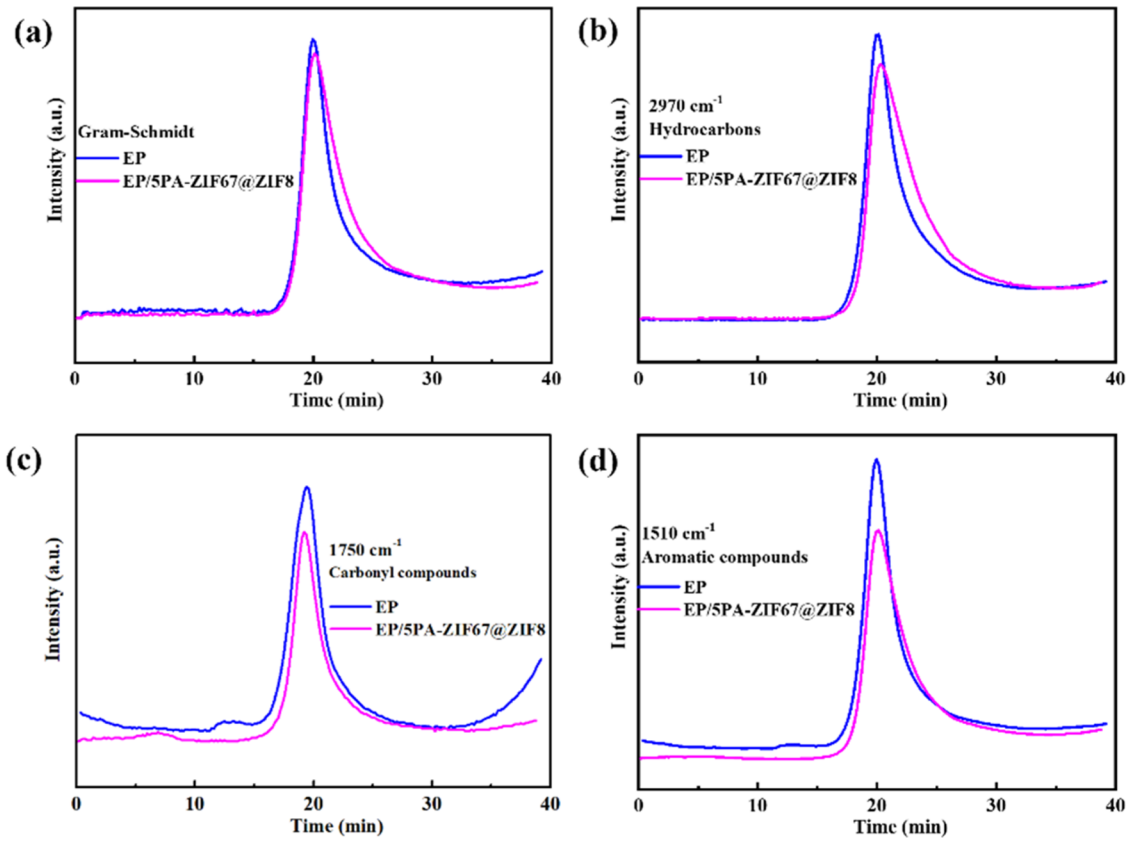

Figure 11. Intensity curves of (a) Gram−Schmidt, (b) hydrocarbons, (c) carbonyl compounds, and (d) aromatic compounds for EP and EP/5PA-ZIF67@ZIF8.

Scheme 2. Proposed Fire Retardancy Mechanism of EP/5PA-ZIF67@ZIF8

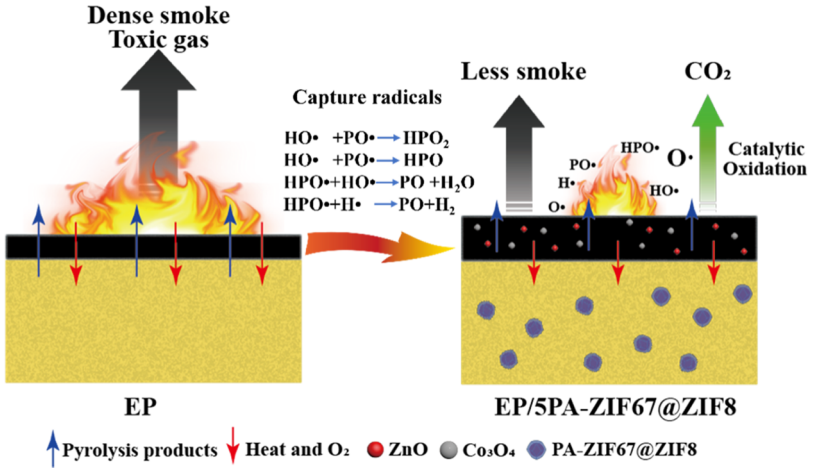

incorporation of PA-ZIF67@ZIF8 can reduce the yield of gaseous products and thus enhance the fire retardancy of the polymeric matrix.

3.7. Flame Retardancy Mechanism. Based on the results of the study, the possible flame retardancy mechanism of PA-ZIF67@ZIF8 is proposed in Scheme 2. PA-ZIF67@ZIF8 generates phosphorous radicals ($PO^{\bullet}$ and $HPO^{\bullet}$) to capture the highly active free radicals ($H^{\bullet}$ and $HO^{\bullet}$) to interrupt the burning process, thus suppressing flame development in the gas phase.[27,29,32] Meanwhile, phosphoric acid derivatives, ZnO, and Co_3O_4 are generated in the solid phase, produced by early-stage pyrolysis of EP/5PA-ZIF67@ZIF8, and promote dehydration and carbonization of the matrix to improve the yield and quality of residual carbon in the thermoset.[27,33] The generated compact residual carbon can exert the flame-retardant effect by isolating the matrix from heat and oxygen.

4. CONCLUSIONS

In this work, ZIF67@ZIF8-PA hybrids with core−shell structures are successfully synthesized. Then, ZIF67@ZIF8-PA hybrids as a flame retardant nanofiller are added to the EP matrix by a physical blending method. With the introduction of 5.0 wt % of ZIF67@ZIF8-PA into EP, the PHRR, TSP, and PCOP are dramatically decreased by 42.2, 27.2, and 41.5%

https://doi.org/10.1021/acsomega.2c01545
ACS Omega 2022, 7, 21664−21674

compared with that of neat EP, respectively. Meanwhile, the LOI value is improved from 25.4 to 29.3%. This is mainly due to the catalytic charring performance of Co_3O_4, ZnO, and phosphorus-containing compounds generated in the burning process of EP/SPA-ZIF67@ZIF8. This work proposed halogen-free flame retardants to effectively reduce the fire hazard of EP.

■ ASSOCIATED CONTENT

Supporting Information

The Supporting Information is available free of charge at https://pubs.acs.org/doi/10.1021/acsomega.2c01545.

Detailed characterization, TEM images of ZIF67@ZIF8 and PA-ZIF67@ZIF8 (Figure S1), storage modulus and tan delta of EP and its composites as a function of temperature (Figure S2), TCOP curves of EP and its nanocomposites (Figure S3), and XRD spectra of char residue of EP/SPA-ZIF67@ZIF8 (Figure S4) (PDF)

■ AUTHOR INFORMATION

Corresponding Authors

Dongdong Yao − *School of Chemistry and Chemical Engineering, Northwestern Polytechnical University, Xi'an 710129, People's Republic of China*; Email: yaodd@nwpu.edu.cn

Yaping Zheng − *School of Chemistry and Chemical Engineering, Northwestern Polytechnical University, Xi'an 710129, People's Republic of China*; orcid.org/0000-0003-4650-6624; Email: zhengyp@nwpu.edu.cn

Authors

Hongni Wang − *School of Chemistry and Chemical Engineering, Northwestern Polytechnical University, Xi'an 710129, People's Republic of China*

Xiaoqian Li − *School of Chemistry and Chemical Engineering, Northwestern Polytechnical University, Xi'an 710129, People's Republic of China*

Fangfang Su − *School of Chemistry and Chemical Engineering, Northwestern Polytechnical University, Xi'an 710129, People's Republic of China*

Jinliang Xie − *School of Chemistry and Chemical Engineering, Northwestern Polytechnical University, Xi'an 710129, People's Republic of China*

Yangyang Xin − *School of Chemistry and Chemical Engineering, Northwestern Polytechnical University, Xi'an 710129, People's Republic of China*

Weirui Zhang − *School of Chemistry and Chemical Engineering, Northwestern Polytechnical University, Xi'an 710129, People's Republic of China*

Chen Liu − *School of Chemistry and Chemical Engineering, Northwestern Polytechnical University, Xi'an 710129, People's Republic of China*

Complete contact information is available at: https://pubs.acs.org/10.1021/acsomega.2c01545

Notes

The authors declare no competing financial interest.

■ ACKNOWLEDGMENTS

This work is supported by the Aeronautical Science Foundation of China (No. 2018ZF53065), the Key Project of Shaanxi Provincial Natural Science Foundation (No. 2021JZ-09), and the National Undergraduate Training Program for Innovation and Entrepreneurship (No. 201910699113). The authors also thank the Analytical & Testing Center of NPU for SEM, XPS, and TEM testing.

■ REFERENCES

(1) Liu, S.; Chevali, V. S.; Xu, Z.; Hui, D.; Wang, H. A review of extending performance of epoxy resins using carbon nanomaterials. *Composites, Part B* **2018**, *136*, 197−214.

(2) Zhou, Y.; Feng, J.; Peng, H.; Qu, H. Q.; Hao, J. W. Catalytic pyrolysis and flame retardancy of epoxy resins with solid acid boron phosphate. *Polym. Degrad. Stab.* **2014**, *110*, 395−404.

(3) Müller, P.; Morys, M.; Sut, A.; Jager, C.; Illerhaus, B.; Schartel, B. Melamine poly (zinc phosphate) as flame retardant in epoxy resin: decomposition pathways, molecular mechanisms and morphology of fire residues. *Polym. Degrad. Stab.* **2016**, *130*, 307−319.

(4) Hu, X.; Yang, H.; Jiang, Y.; He, H.; Liu, H.; Huang, H.; Wan, C. Facile synthesis of a novel transparent hyperbranched phosphorous/nitrogen-containing flame retardant and its application in reducing the fire hazard of epoxy resin. *J. Hazard. Mater.* **2019**, *379*, No. 120793.

(5) Tran, P.; Nguyen, Q. T.; Lau, K. T. Fire performance of polymer-based composites for maritime infrastructure. *Composites, Part B* **2018**, *155*, 31−48.

(6) Wang, X.; Xing, W. Y.; Feng, X. M.; Yu, B.; Lu, H. D.; Song, L.; Hu, Y. The effect of metal oxide decorated graphene hybrids on the improved thermal and the reduced smoke toxicity in epoxy resins. *Chem. Eng. J.* **2014**, *250*, 214−220.

(7) Wang, H. W.; Qiao, H.; Guo, J.; Sun, J.; Li, H. F.; Zhang, S.; Gu, X. Y. Preparation of cobalt-based metal organic framework and its application as synergistic flame retardant in thermoplastic polyurethane (TPU). *Composites, Part B* **2020**, *182*, No. 107498.

(8) Zhou, H. C.; Long, J. R.; Yaghi, O. Introduction to metal-organic frameworks. *Chem. Rev.* **2012**, *112*, 673−674.

(9) Hou, Y. B.; Hu, W. Z.; Gui, Z.; Hu, Y. Preparation of metal-organic frameworks and their application as flame retardants for polystyrene. *Ind. Eng. Chem. Res.* **2017**, *56*, 2036−2045.

(10) Sai, T.; Ran, S. Y.; Guo, Z. H.; Fang, Z. P. A Zr-based metal organic frameworks towards improving fire safety and thermal stability of polycarbonate. *Composites, Part B* **2019**, *176*, No. 107198.

(11) Guo, W. W.; Nie, S. B.; Kalali, E. N.; Wang, X.; Wang, W.; Cai, W.; Song, L.; Hu, Y. Construction of SiO_2@UiO-66 core-shell microarchitectures through covalent linkage as flame retardant and smoke suppressant for epoxy resins. *Composites, Part B* **2019**, *176*, No. 107261.

(12) Pan, Y. T.; Zhang, Z.; Yang, R. The rise of MOFs and their derivatives for flame retardant polymeric materials: A critical review. *Composites, Part B* **2020**, *199*, No. 108265.

(13) Zhang, M.; Ding, X. Q.; Zhan, Y. X.; Wang, Y. T.; Wang, X. L. Improving the flame retardancy of poly (lactic acid) using an efficient ternary hybrid flame retardant by dual modification of graphene oxide with phenylphosphinic acid and nano MOFs. *J. Hazard. Mater.* **2020**, *384*, No. 121260.

(14) Jing, Z.; Zhi, L.; Qi, X. L.; Zhang, W.; Wang, D.-Y. Size tailored bimetallic metal-organic framework (MOF) on graphene oxide with sandwich-like structure as functional nano-hybrids for improving fire safety of epoxy. *Composites, Part B* **2020**, *188*, No. 107881.

(15) Wang, X. G.; Wang, S. H.; Wang, W. J.; Li, H. F.; Liu, X. D.; Gu, X. Y.; Bourbigot, S.; Wang, Z. W.; Wang, Z.; Sun, J.; Zhang, S. The flammability and mechanical properties of poly(lactic acid) composites containing Ni-MOF nanosheets with polyhydroxy groups. *Composites, Part B* **2020**, *183*, No. 107568.

(16) Xu, W. Z.; Wang, X. L.; Wu, Y.; Li, W.; Chen, C. Y. Functionalized graphene with Co-ZIF adsorbed borate ions as an effective flame retardant and smoke suppression agent for epoxy resin. *J. Hazard. Mater.* **2019**, *363*, 138−151.

(17) Li, A. J.; Xu, W. Z.; Chen, R.; Liu, Y. C.; Li, W. Fabrication of zeolitic imidazolate frameworks on layered double hydroxide

https://doi.org/10.1021/acsomega.2c01545
ACS Omega 2022, 7, 21664−21674

nanosheets to improve the fire safety of epoxy resin. *Composites, Part A* **2018**, *112*, 558−571.
(18) Pan, Y. T.; Wan, J. T.; Zhao, X. L.; Li, C.; Wang, D. Y. Interfacial growth of MOF-derived layered double hydroxide nanosheets on graphene slab towards fabrication of multifunctional epoxy nanocomposites. *Chem. Eng. J.* **2017**, *330*, 1222−1231.
(19) Zhang, J.; Li, Z.; Qi, X. L.; Wang, D. Y. Recent progress on metal−organic framework and its derivatives as novel fire retardants to polymeric materials. *Nano-Micro Lett.* **2020**, *12*, No. 173.
(20) Xu, B. L.; Xu, W. Z.; Wang, G. S.; Liu, L. C.; Xu, J. Zeolitic imidazolate frameworks- 8 modified graphene as a green flame retardant for reducing the fire risk of epoxy resin. *Polym. Adv. Technol.* **2018**, *29*, 1733−1743.
(21) Li, A. J.; Xu, W. Z.; Chen, R.; Liu, Y. C.; Li, W. Fabrication of zeolitic imidazolate frameworks on layered double hydroxide nanosheets to improve the fire safety of epoxy resin. *Composites, Part A* **2018**, *112*, 558−571.
(22) Hou, Y. B.; Qiu, S. L.; Hu, Y.; Kundu, C.; Zhou, G.; Hu, W. Z. Construction of bimetallic ZIF-derived Co-Ni LDHs on the surfaces of GO or CNTs with a recyclable method: toward reduced toxicity of gaseous thermal decomposition products of unsaturated polyester resin. *ACS Appl. Mater. Interfaces* **2018**, *10*, 18359−18371.
(23) Zhang, Z. D.; Li, X. L.; Yuan, Y. S.; Pan, Y. T.; Wang, D. Y.; Yang, R. J. Confined dispersion of zinc Hydroxystannate nanoparticles into layered bimetallic hydroxide nanocapsules and its application in flame-retardant epoxy nanocomposites. *ACS Appl. Mater. Interfaces* **2019**, *11*, 40951−40960.
(24) Zhao, J. J.; Quan, X.; Chen, S.; Liu, Y. M.; Yu, H. T. Cobalt nanoparticles encapsulated in porous carbons derived from core-Shell ZIF67@ZIF8 as efficient electrocatalysts for oxygen evolution reaction. *ACS Appl. Mater. Interfaces* **2017**, *9*, 28685−28694.
(25) Zhao, H. Y.; Wang, Y.; Zhao, L. Magnetic nanocomposites derived from hollow ZIF-67 and core-shell ZIF-67@ZIF-8: synthesis, properties, and adsorption of rhodamine B. *Eur. J. Inorg. Chem.* **2017**, *2017*, 4110−4116.
(26) Huo, S. Q.; Wang, J.; Yang, S.; Wang, J. P.; Zhang, B.; Zhang, B.; Chen, X.; Tang, Y. S. Synthesis of a novel phosphorus-nitrogen type flame retardant composed of maleimide, triazine-trione, and phosphaphenanthrene. *Polym. Degrad. Stab.* **2016**, *131*, 106−113.
(27) Chi, Z. Y.; Guo, Z. W.; Xu, Z.; Zhang, M. J.; Li, M.; Shang, L.; Ao, Y. H. A DOPO-based phosphorus-nitrogen flame retardant bio-based epoxy resin from diphenolic acid: Synthesis, flame-retardant behavior and mechanism. *Polym. Degrad. Stab.* **2020**, *176*, No. 109151.
(28) Qu, Z. C.; Kun, W.; Meng, W. H.; Nan, B. F.; Hu, Z. R.; Xu, C. -A.; Tan, Z. Y.; Zhang, Q.; Meng, H. F.; Shi, J. Surface coordination of black phosphorene for excellent stability, flame retardancy and thermal conductivity in epoxy resin. *Chem. Eng. J.* **2020**, *397*, No. 125416.
(29) Qiu, S. L.; Ma, C.; Wang, X.; Zhou, X.; Feng, X. M.; Yuen, R. K. K.; Hu, Y. Melamine-containing polyphosphazene wrapped ammonium polyphosphate: A novel multifunctional organic-inorganic hybrid flame retardant. *J. Hazard. Mater.* **2018**, *344*, 839−848.
(30) Wang, J. L.; Zhang, D. C.; Zhang, Y.; Cai, W.; Yao, C. X.; Hu, Y.; Hu, W. Z. Construction of multifunctional boron nitride nanosheet towards reducing toxic volatiles (CO and HCN) generation and fire hazard of thermoplastic polyurethane. *J. Hazard. Mater.* **2019**, *362*, 482−494.
(31) Qiu, S. L.; Hou, Y. B.; Xing, W. Y.; Ma, C.; Zhou, X.; Liu, L. X.; Kan, Y. C.; Yuen, R. K. K.; Hu, Y. Self-assembled super molecular aggregate supported on boron nitride nanoplatelets for flame retardant and friction application. *Chem. Eng. J.* **2018**, *349*, 223−234.
(32) Zhang, J.; Li, Z.; Zhang, L.; Yang, Y. X.; Wang, D. Y. Green synthesis of biomass phytic acid-functionalized UiO-66-NH_2 hierarchical hybrids toward fire safety of epoxy resin. *ACS Sustainable Chem. Eng.* **2020**, *8*, 994−1003.
(33) Nabipour, H.; Wang, X.; Song, L.; Hu, Y. Metal organic frameworks for flame retardants polymers application: a critical review. *Composites, Part A* **2020**, *139*, No. 106113.
(34) Sai, T.; Ran, S. Y.; Guo, Z. H.; Yan, H.; Zhang, Y.; Song, P. G.; Zhang, T.; Wang, H.; Fang, Z. P. Deposition growth of Zr-based MOFs on cerium phenylphosphonate lamella towards enhanced thermal stability and fire safety of polycarbonate. *Composites, Part B* **2020**, *197*, No. 108064.
(35) Xiong, Z. Q.; Zhang, Y.; Du, X. Y.; Song, P. G.; Fang, Z. P. Green and scalable fabrication of core−shell biobased flame retardants for reducing flammability of polylactic acid. *ACS Sustainable Chem. Eng.* **2019**, *7*, 8954−8963.
(36) Xu, W. Z.; Wang, X. L.; Liu, Y. C.; Li, W.; Chen, R. Improving fire safety of epoxy filled with graphene hybrid incorporated with zeolitic imidazolate framework/layered double hydroxide. *Polym. Degrad. Stab.* **2018**, *154*, 27−36.

https://doi.org/10.1021/acsomega.2c01545
ACS Omega 2022, 7, 21664−21674